

Actively Stabilized Model Rocket Simulator

Technical Documentation

Guido di Pasquo¹

¹ Aerospace Engineering student at “Universidad Tecnológica Nacional – Regional Haedo”. Buenos Aires, Argentina.
guidodipasquo@gmail.com

Contents

List of symbols and abbreviations.....	3
1. Introduction.....	5
2. PID Tuner Underlying Model.....	5
2.1 Model Rocket Equations of Motion.....	5
2.2 Implementation of the Rocket's Aerodynamics.....	6
2.2.1 Body Aerodynamics.....	8
2.2.1.1 Barrowman Equations.....	8
2.2.1.2 Body Lift.....	9
2.2.1.3 Body Pitch Damping Factor.....	10
2.2.2 Fin Aerodynamics.....	10
2.2.2.1 Two-dimensional coefficients.....	10
2.2.2.2 Tridimensional Coefficients.....	13
Attached and detached fins.....	13
Diederich Semi-Empirical Method.....	14
Fin-Body Interference.....	15
2.3 Actuator Dynamics.....	15
2.4 Wind.....	17
2.5 PID Tuner Code.....	17
3. Graphic Representation.....	18
3.1 Colour of the Force Application Point in the Canvas.....	18
3.2 Tridimensional Graphics.....	19
4. Conclusion.....	20
Bibliography.....	21

List of symbols and abbreviations.

Symbols

α	Angle of attack
A_{ref}	Reference area of the rocket
A_{plan}	Planar area of the component
A_{fin}	Planar area of the fin
AR	Aspect ratio
C_l	Bidimensional lift coefficient
C_d	Bidimensional drag coefficient
C_n	Bidimensional normal force coefficient
C_a	Bidimensional axial coefficient
C_{n_α}	Bidimensional normal force coefficient slope, $\frac{\partial C_n}{\partial \alpha}$
C_N	Tridimensional normal force coefficient
C_A	Tridimensional axial force coefficient
C_M	Moment coefficient calculated from the centre of gravity
C_{N_α}	Tridimensional normal force coefficient slope, $\frac{\partial C_N}{\partial \alpha}$
δ_e	Actuator deflection (radians)
F_n	Force acting in the n axis
g_n	Gravity component in the n axis
I_n	Mass Moment of Inertia along the n axis
$K_{T(B)}$	Body-fin interference correction factor
M_n	Moment acting in the n axis
M_Q	Pitch damping factor
m	Mass
\dot{n}	Time derivative of the magnitude n

List of symbols and abbreviations.

Q	Angular velocity in the Y axes (pitch velocity)
q	Dynamic pressure
R_B^G	Body frame to global frame rotation matrix
R_G^B	Global frame to body frame rotation matrix
ρ	Air density
S	Reference area
T	Thrust
θ	Pitch angle (measured from the, vertical, X axis)
U	Local velocity in the X axis (longitudinal)
V_{cg}	Velocity of the centre of mass
W	Local velocity in the Z axis (transversal)
x_t	Position of the motor mount (measured from the tip of the nose cone)
x_{cg}	Position of the centre of gravity (measured from the tip of the nose cone)

Abbreviations

AoA	Angle of attack
cg	Centre of gravity
PID	Proportional Integral Derivative (controller)
TVC	Thrust Vector Control

1. Introduction.

Since there has been an increase in model rockets with active control systems, mainly in the form of TVC, the question of how to tune a PID has arisen. The fundamental problem in PID tuning for model rockets is the cost of in-plant tuning, since each iteration, or flight, needs of a new motor, in addition to the risk of destroying the model in the process. For this reason, a simple, semi-plug and play, Python-based, manual tuner has been developed, which enables the simulation of model rockets with active control systems, be it in the form of TVC or active fin control. Basic Software in the Loop capabilities were included to expand the scope of the simulator beyond the included controller.

2. PID Tuner Underlying Model.

2.1 Model Rocket Equations of Motion.

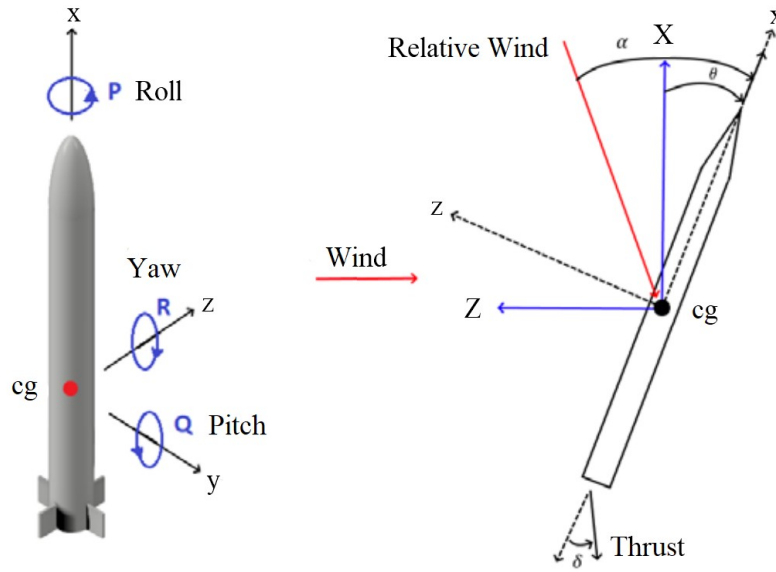


Figure 2.1: Diagram of a model rocket.

The first step is to find the equations of motion for pitch in a model rocket, which are the following:

$$\begin{aligned}\sum F_x &= m \dot{U} \\ \sum F_z &= m \dot{W} \\ \sum M_x &= I_y \dot{Q}\end{aligned}\tag{2.1}$$

Where m its mass and I_y its moment of inertia.

Note that there are not vector derivatives. This arises from the simulation method, where the velocity is considered a global magnitude. The local accelerations are integrated within the local frame, which returns the local perturbation velocities. The global velocity is transformed into the

local frame, after which the local perturbation velocities are added to it. Lastly, the total local velocity is transformed back into the global frame. This transformation is done in each time step of the simulation, using a new θ each time.

The rotational matrices are:

$$R_B^G = \begin{pmatrix} \cos(\theta) & \sin(\theta) \\ -\sin(\theta) & \cos(\theta) \end{pmatrix} \quad (2.2)$$

$$R_G^B = [R_B^G]^T = \begin{pmatrix} \cos(\theta) & -\sin(\theta) \\ \sin(\theta) & \cos(\theta) \end{pmatrix}$$

Where R_B^G transforms a vector from the body frame into the global frame, and R_G^B transforms a vector from the global frame into the body frame. Note that θ is the pitch angle.

Expanding the left-hand side of Eq.2.1:

$$\begin{aligned} \sum F_x &= T \cos(\delta_e) + m g_x - q S \cdot C_A \\ \sum F_z &= T \sin(\delta_e) + m g_z + q S \cdot C_N \\ \sum M_y &= T \sin(\delta_e)(x_t - x_{cg}) + q S d \cdot C_M - 0.2 \rho Q^2 M_Q \end{aligned} \quad (2.3)$$

Where S is the maximum cross-sectional area of the rocket, q the dynamic pressure, ρ the density², α the angle of attack, δ_e the TVC angle (in radians), and T is the thrust of the motor. C_N is the normal force coefficient, C_A is the axial force coefficient, C_M the moment coefficient referenced to the centre of mass, M_Q the body's pitch damping factor, and g the gravitational acceleration in the body frame. x_{cg} is the distance from the tip of the nose cone to the centre of mass, and x_t to the TVC mount. In case of using active control fins³, δ_e is set to the initial offset angle of the motor.

2.2 Implementation of the Rocket's Aerodynamics.

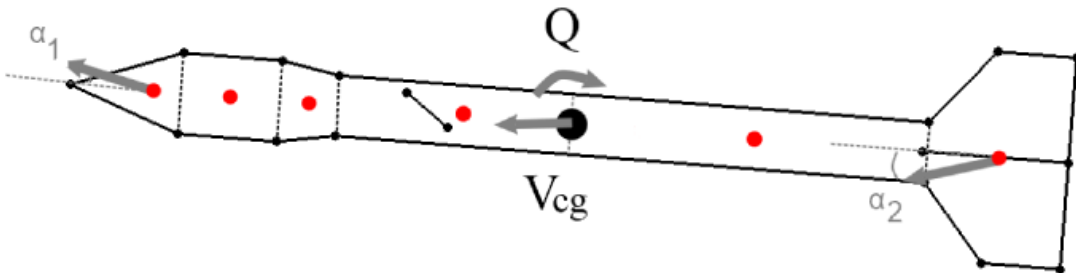


Figure 2.2: Velocity of each component.

² The atmospheric parameters vary with altitude following the International Standard Atmosphere model.

³ The influence of the control fin is calculated in the aerodynamic coefficients.

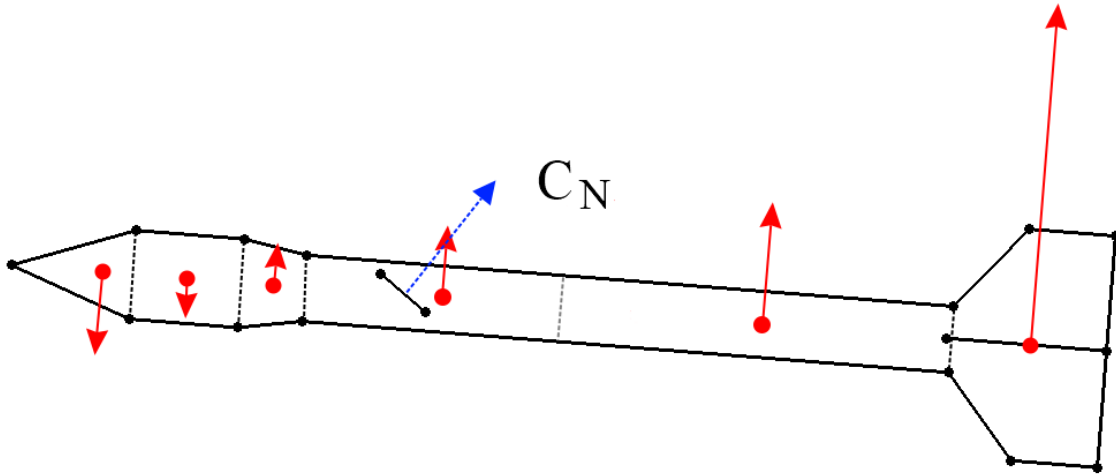


Figure 2.3: Normal force generated by each component.

The basic simulation procedure is the following:

1. Separate⁴ the rocket in the basic components that conform the body and the fins, as in Figure 2.2.
2. Compute the geometric parameters of the fins.
3. Compute the approximate pitch damping coefficient of the body. It is worth noting that its effects are appreciable only in maneuvers that induce high pitching velocities, for example, unstable TVC rockets after burnout.
4. Use last time step θ to transform the global velocity of the rocket into V_{cg} (local coordinates).
5. Use V_{cg} and Q to obtain the velocity of each component, note that supersonic flow is not supported and the simulator is not intended to be used for velocities above $M=0.6$.
6. Calculate the Angle of Attack of each component.
7. Calculate the normal force coefficient of each body component using the Extended Barrowman Equations.
8. Compute the normal force coefficient of the fins using Diederich Semi-Empirical Method.
9. Calculate the fin-body interference if needed.
10. Decompose the normal force coefficient of the control fin into body referenced C_N and C_A .
11. Compute the dynamic pressure scaling coefficient $\frac{V_{component}^2}{V_{cg}^2}$ to apply to the C_N of each component.
12. Compute the total C_N .
13. Calculate the position of the centre of pressure.

⁴ The component that contains the centre of mass must be separated in two.

14. Compute the moment coefficient using the centre of mass as reference. Note that is not necessary to calculate the pitch damping coefficient of the fins since its effect is already included in the modified AoA along the length of the rocket due to Q.
15. Compute the axial force coefficient of the body as in [1]⁵.
16. Add the axial force coefficient of the fins to the body C_A .
17. Compute Eq.2.3, Eq.2.1 and integrate the latter's result.
18. Transform Eq.2.1 results and their integrations into global coordinates and add them to the global magnitudes.
19. Repeat steps 4 through 18 for each time step.

2.2.1 Body Aerodynamics.

The aerodynamics of the rocket body are computed with the Extended Barrowman Equations developed by Barrowman and Galejs. In both cases, the centre of pressure of each component is assumed to be located in the centre of its planform area.

2.2.1.1 Barrowman Equations

Barrowman's method [2] consists in splitting the rocket's body into simple components (nose shapes, circular cylinders, and conical frustums), for which the normal force coefficient can be readily calculated. Afterwards, the results are recombined to obtain the total vehicle solution.

The assumptions made by the derivation are:

- The angle of attack is small.
- The flow is steady and irrotational.
- The vehicle is a rigid body.
- The nose tip is a sharp point.
- The vehicle body is slender and axially symmetric.

The steady state running normal load in the assumed bodies is, for subsonic flow:

$$n(x) = \rho V \frac{\partial}{\partial x} [A(x)w(x)] \quad (2.4)$$

Where $A(x)$ is the cross-sectional area of the body and $w(x)$ is the rigid body downwash,

$$w(x) = V \sin(\alpha) \quad (2.5)$$

By combining 2.5 with 2.4 and replacing in the definition of normal force coefficient, one can integrate along the body's length to obtain,

$$C_N = \frac{2\sin(\alpha)}{A_{ref}} [A(l_0) - A(0)] \quad (2.6)$$

Where A_{ref} is the maximum cross-sectional area of the rocket.

5 The fins are assumed to have rounded leading and trailing edges and a thickness of 3mm.

2.2.1.2 Body Lift.

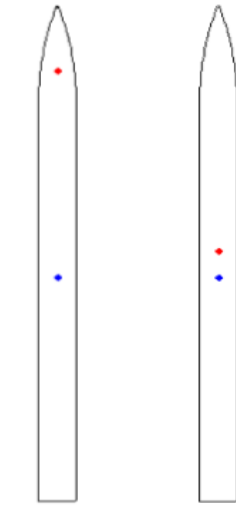


Figure 2.4: Example of the effect of body lift on the C_p location, showing the C_p at $\alpha = 0^\circ$ (left) and $\alpha = 90^\circ$ (right).

Eq.2.6 neglects body lift. However, in the flight of long, slender rockets, as well as for most rockets at high angles of attack⁶, the lift might be considerable, usually shifting the centre of pressure towards the geometric centre of the rocket, which will affect its stability (or lack of thereof).

To solve the issue, Robert Galejs [3] suggested adding a correction term in the form of,

$$C_N = K \frac{A_{plan}}{A_{ref}} \sin^2(\alpha) \quad (2.7)$$

Where A_{plan} is the planar area of the component, and K is a constant ranging from $K \approx 1.1$ to $K \approx 1.5$, where the lower value is used.

The total normal force coefficient produced by each body component can be expressed as the sum of Eq.2.6 and Eq.2.7,

$$C_{N_i} = \frac{2 \sin(\alpha_i)}{A_{ref}} [A(l_0)_i - A(0)_i] + K \frac{A_{plan_i}}{A_{ref}} \sin^2(\alpha_i) \quad (2.8)$$

⁶ Although the Barrowman Equations establish low AoA, by adding the effects of body lift and not approximating $\sin(\alpha) \simeq \alpha$, it is assumed that the final result at high AoA is sufficiently accurate for the scope of the simulator.

2.2.1.3 Body Pitch Damping Factor.

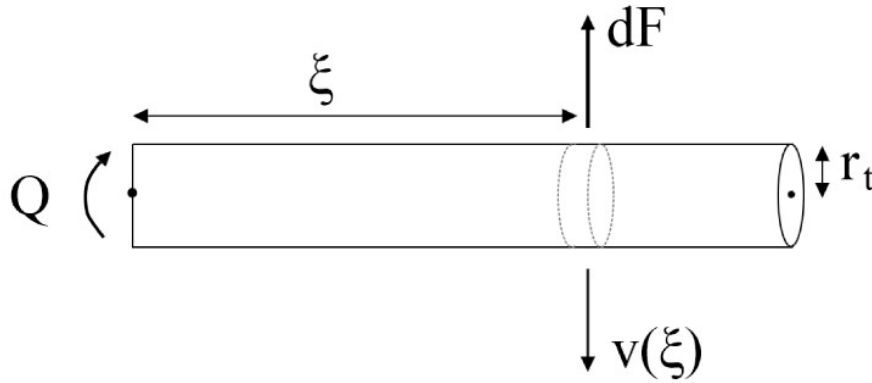


Figure 2.5: Pitch damping moment due to a pitching body component.

The change in AoA and dynamic pressure along the rocket's length does not provide realistic damping at low velocities and high Q . Consequently, the pitch damping moment [1] produced by the approximate drag of the rocket's body rotating along the Y-axis in still air is added to the movement equations. It is then scaled by 0.2 to avoid unrealistic over-damping during the flight.

A cylinder in perpendicular flow has a drag coefficient of approximately $C_D=1.1$, with the reference area being the planform area of the cylinder. Therefore, the force produced by a short piece of cylinder of length $d\xi$ at a distance ξ from the centre of mass, as shown in Figure 2.5, is

$$dF = 1.1 \cdot \frac{1}{2} \rho (Q\xi)^2 \cdot 2r_t d\xi \quad (2.9)$$

Where $2r_t d\xi$ is the reference area of the cylinder differential. The associated moment is $dM = \xi dF$. Integrating from 0 to l yields the total pitching moment of the component,

$$M = 0.275 \cdot \rho r_t l^4 Q^2 \quad (2.10)$$

In consequence, the pitch damping factor of Eq.2.3 can be readily calculated as,

$$M_Q = 0.275 \cdot r_t l^4 \quad (2.11)$$

2.2.2 Fin Aerodynamics.

Although most rocket fins are flat plates, there is not much information about their behaviour through a large range of angles of attack. Consequently, they are assumed to be made out of a NACA-0009 airfoil due to the availability of wind tunnel data for it [4].

2.2.2.1 Two-dimensional coefficients.

Two elements must be pointed out about Figure 2.6. Firstly, the airfoil, unlike the flat plate, is not symmetrical along the Z-axis. The effects of this asymmetry can be seen in the behaviour of the C_l for AoAs greater than 90° . This is modified in the simulator to ensure symmetry. Secondly, the stall is removed from the dataset. The reason for this modification is that the simulator computes the tridimensional lift coefficient using Diederich semi-empirical method, which cannot predict the tridimensional stall of the fin. In addition, the tridimensional stall for small aspect ratio wings

occurs at much greater angles of attacks than the bidimensional stall, reason why a drop in C_N at 8° to 10° AoA would not be realistic, and it is preferred to remove the airfoil stall altogether.

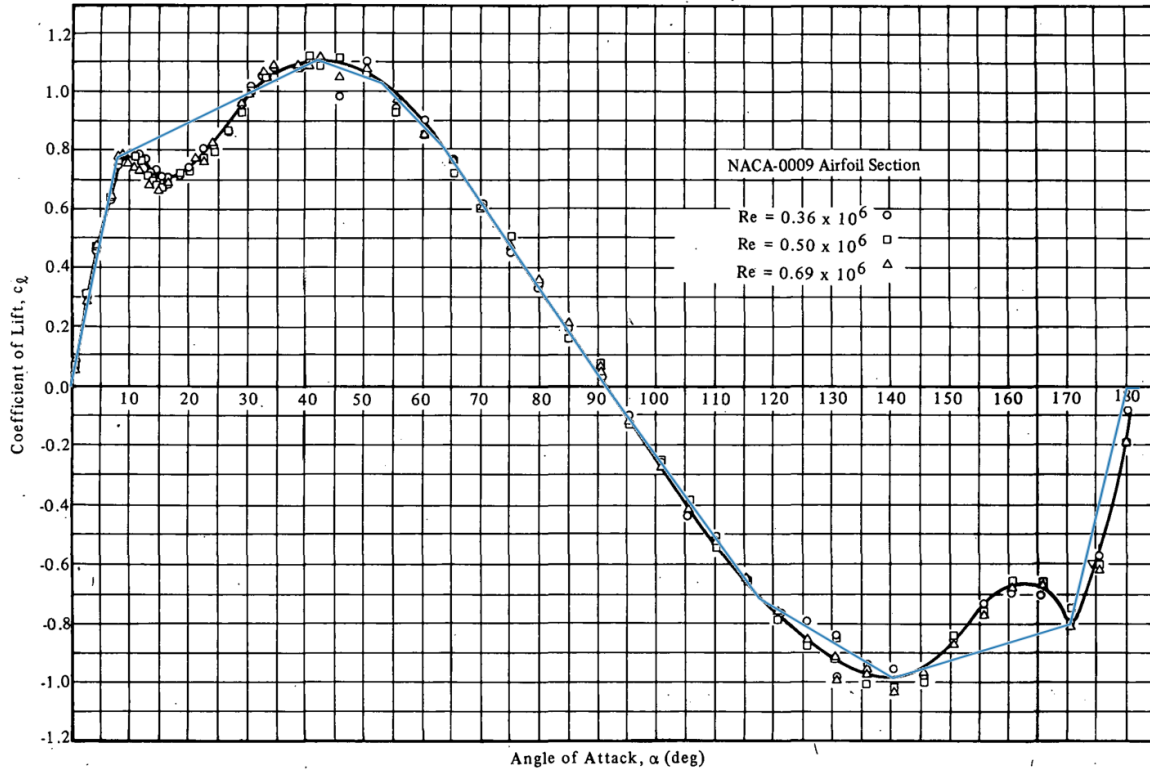


Figure 2.6: Full Range Section Lift Coefficients for the NACA-0009 Airfoil and its implementation in the simulator.

The drag coefficient data in Figure 2.7 is also modified. In this case, the low C_d at low AoA is increased to match the C_d at near 180° AoA since it is assumed that the drag associated with a sharp trailing edge acting as leading edge is more resembling of the drag of a flat plate rather than that of the airfoil in its standard configuration.

The C_n and C_a are obtained by rotating the resultant aerodynamic forces,

$$\begin{aligned} C_n &= C_l \cos(\alpha) + C_d \sin(\alpha) \\ C_a &= -C_l \sin(\alpha) + C_d \cos(\alpha) \end{aligned} \quad (2.12)$$

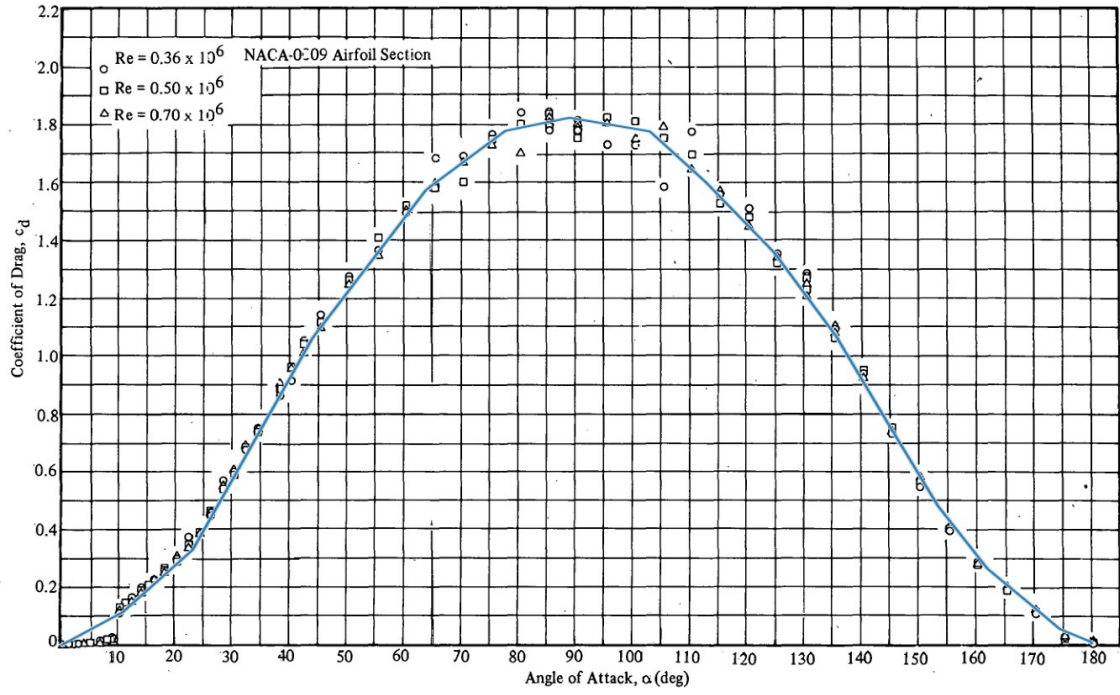


Figure 2.7: Full Range Section Drag Coefficients for the NACA-0009 Airfoil and its implementation in the simulator.

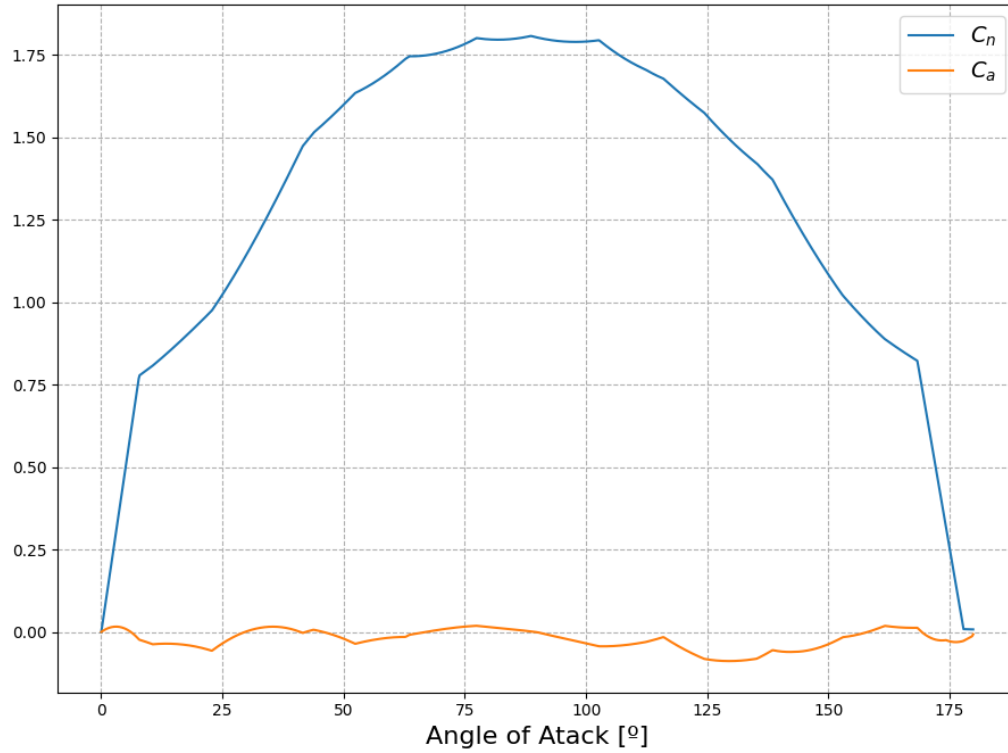


Figure 2.8: Implementation of the Full Range Section Normal Force and Axial Force Coefficient for a flat plate.

The normal force slope C_{n_α} is calculated as,

$$C_{n_\alpha} = \frac{C_n}{\alpha} \quad (2.13)$$

2.2.2.2 Tridimensional Coefficients.

Attached and detached fins.

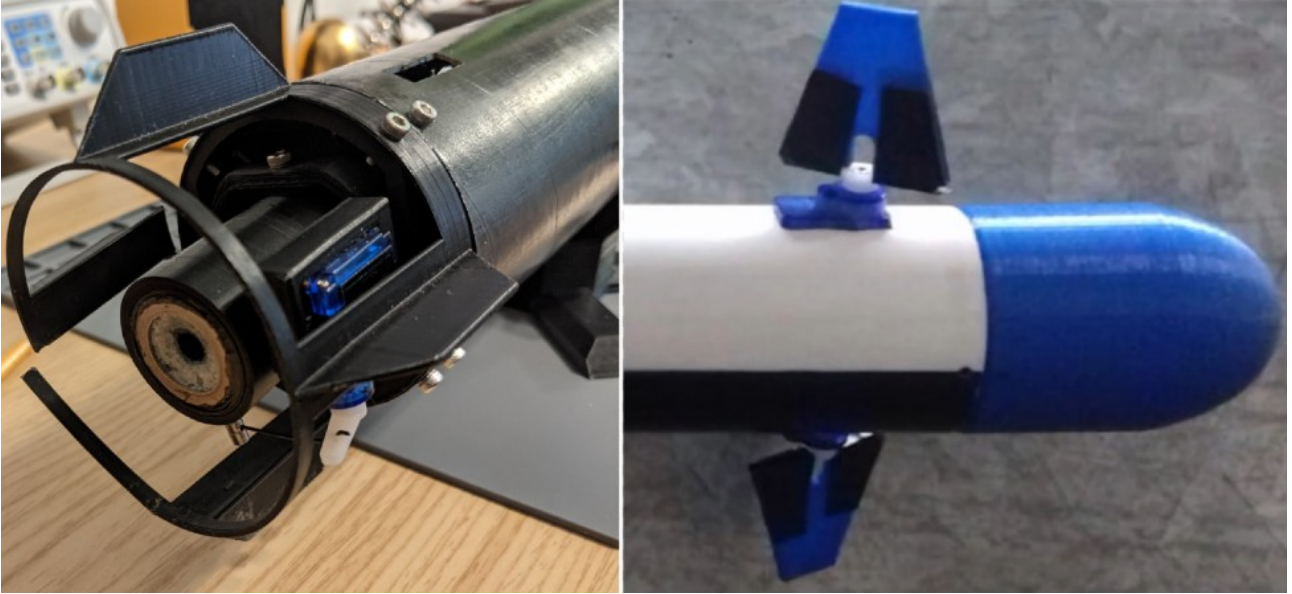


Figure 2.9: Example of detached fins, from Peregrine Developments and ZPC Rocket Team.

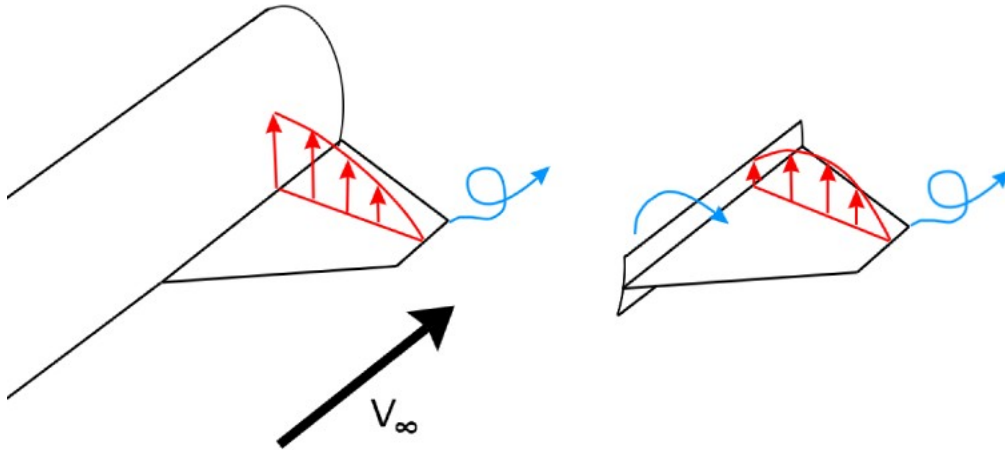


Figure 2.10: Comparison of the lift distribution between Attached (left) and Detached (right) fins.

In the example of the left of Figure 2.10, one can see why the aspect ratio is computed as double the aspect ratio of the isolated fin, with b and A_{fin} being its wingspan and plan area,

$$AR = 2 \frac{b^2}{A_{fin}} \quad (2.14)$$

However, in case the fin is detached from the main body, it does not act as a half wing. In consequence, the AR must be modified to better match the lift generated.

Is assumed that the piece of body where the fin is attached acts as an end plate [5] of $0.2 h/b$, and the following correction coefficient is proposed,

$$AR_{detached} = AR_{attached} \cdot [1 - (r/2)] \quad (2.15)$$

Being r the correction factor $r = 0.75$, obtained from [5]:

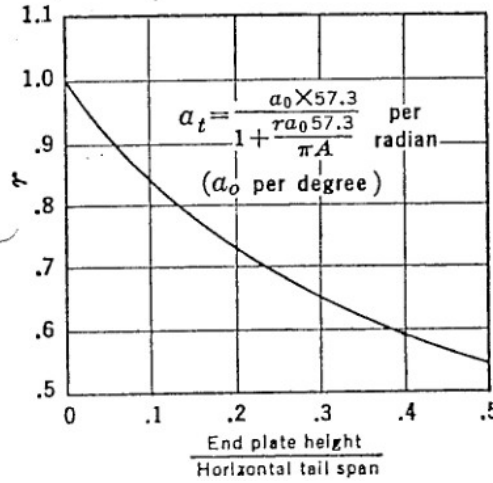


Figure 2.11: Correction factor r function of h/b

One must remember that this end plate acts not to increase the aspect ratio, and consequently the lift slope, but to mitigate its reduction. Additionally, and unlike the end plates in [5], it affects only the wing root, leaving the tip unaltered.

The correction coefficient proposed is valid at the extremes. At $r = 1$ (no end plate), the aspect ratio is that of one isolated fin (1/2 of the calculated aspect ratio). At $r = 0$ (fin attached to the body), the aspect ratio is that of a hypothetical wing of $b_{wing} = 2 b_{fin}$ (calculated in 2.14). In

addition, the correction factor is valid in case the fin is separated from the body by a servo or rod (Figure 2.9, right), accounting for the increase in lift the body produces, but not going to the extent of calculating it as if it was attached.

By replacing the value of r in Eq.2.15, the value of the final AR of the detached fin can be obtained,

$$AR_{detached} = 0.625 AR_{attached} \quad (2.16)$$

Diederich Semi-Empirical Method.

After the AR is calculated, the tridimensional C_{N_α} is obtained using Diederich Semi-Empirical Method [6] for compressible subsonic flow,

$$C_{n_{\alpha} \text{ Compressible}} = \frac{C_{n_{\alpha}}}{\sqrt{1 - M^2 \cos^2 \Lambda}} \quad (2.17)$$

$$C_{N_\alpha} = \frac{F}{F \sqrt{1 + \frac{4}{F^2} + 2}} C_{n_{\alpha} \text{ Compressible}} \quad (2.18)$$

Where Λ is the sweepback angle measured from the 25% chord, and

$$F = \frac{AR}{\eta \cos \Lambda} \quad (2.19)$$

$$\eta = \frac{C_{n_{\alpha} \text{ Compressible}}}{2 \pi} \quad (2.20)$$

The C_{N_α} is then scaled by

$$\frac{2 A_{fin}}{A_{ref}} \quad (2.21)$$

The disadvantage of using Diederich method is that the results are not accurate for large AoA, mainly at 90°. One would find that the C_N of the fin converges to the bidimensional C_n with increasing AR , while it will drop considerably below the tridimensional value of flat plates for low AR .

The axial force coefficient is not corrected for tridimensional effects, therefore, the bidimensional one, scaled by Eq.2.21, is used. In addition, the induced drag produced by the fins is not calculated and is neglected in the simulation, which will produce higher velocities in the simulated flight than in the real one. Nonetheless, for most cases, the stability of the real model should not be compromised.

Fin-Body Interference.

The mayor interference effects encountered on the studied rockets are the change in normal force of the fin alone when it is brought into the presence of the body and the change of normal force on the body between the fins [7]. They are handled by the use of a correction factor applied only to the fin⁷.

$$(C_{N_\alpha})_{T(B)} = K_{T(B)} C_{N_\alpha Fin} \quad (2.22)$$

Where $(C_{N_\alpha})_{T(B)}$ is the normal force coefficient slope of the fins in the presence of the body and $K_{T(B)}$ is calculated as,

$$K_{T(B)} = 1 + \frac{r_t}{b_{fin} + r_t} \quad (2.23)$$

where r_t is the radius of the body at the fin.

2.3 Actuator Dynamics.

The actuator dynamics may have a detrimental effect in stability, therefore they must be modelled. The transfer function of the servo is extracted from experimental data from [8]. Due to the non-linear actuator dynamics the transfer function proposed is:

$$\frac{K}{s^2 + J \cdot s + K} \quad (2.24)$$

Where K and J vary with the relative magnitude of the inputs.

⁷ The fin-body interference is computed only for attached fins.

Actuator Dynamics.

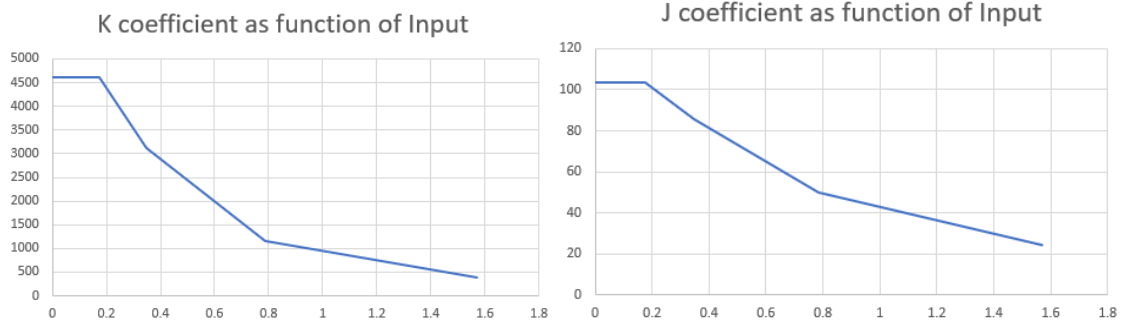


Figure 2.12 – K and J as a function of relative input (radians).

The relative magnitude of the inputs refers to the difference between an input and the current position of the servo, is easy to see that an input from 40° to 45° is equivalent to a 5° input (or “*u_delta*”) in the simulator.

The resulting State Space Model is,

$$\begin{pmatrix} \dot{\delta} \\ \ddot{\delta} \end{pmatrix} = \begin{pmatrix} 0 & 1 \\ -K & -J \end{pmatrix} \begin{pmatrix} \delta \\ \dot{\delta} \end{pmatrix} + \begin{pmatrix} 0 \\ K \end{pmatrix} u$$

where C is assumed to be the Identity matrix, D is zero, and K and J are calculated with a trend line that spans from 10° to 90°. The Tustin discretization [9] is done in the program and the resulting discrete state space model is used to compute the actuator displacement. The simulated response is slightly faster than the experimental due to the relative input decreasing during the movement of the actuator. However, it is adjusted by multiplying “*u_delta*” by a factor of 1.45 to simulate the unloaded servo, or by 2.1 to simulate the TVC mount inertia.

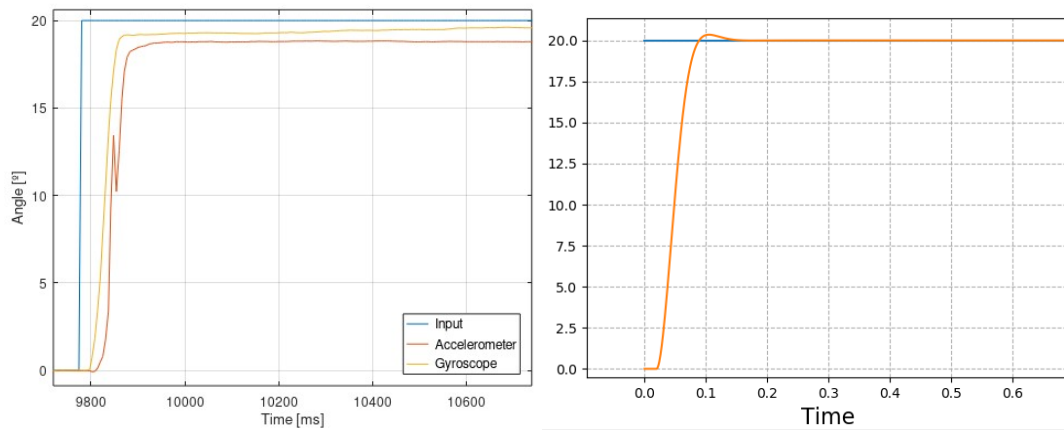


Figure 2.13 – Verification of the servo. Left is the experimental data from [8] and Right is the simulation of the program.

The error was not modelled due to its random nature [8], the rise time in both cases is 0.069 seconds. The sample time delay can be seen in both plots, the main difference in the responses is the slight overshoot seen in the simulation.

The *Servo* class in *servo_lib.py* contains a test function, where, after setting up the servo, one can test any input and correct the compensation factor accordingly.

```
servo = servo_lib.Servo()
servo.setup(actuator_weight_compensation=1.45, definition=1, servo_s_t=0.02)
servo.test(u_deg=30)
```

Figure 2.14: Example of the test method for the actuator dynamics.

2.4 Wind.

The wind gust velocity is calculated using the *wind gust* parameter as the standard deviation of a normal distribution with mean 0. The obtained gust is then added to the set wind speed. The velocity of the gust is updated every 100 ms.

2.5 PID Tuner Code.

The details of the code will not be shown, instead the overall behaviour is analysed, followed by key points that must be taken into account when translating the gains obtained to a flight computer.

First, the block diagram of the default controller is analysed:

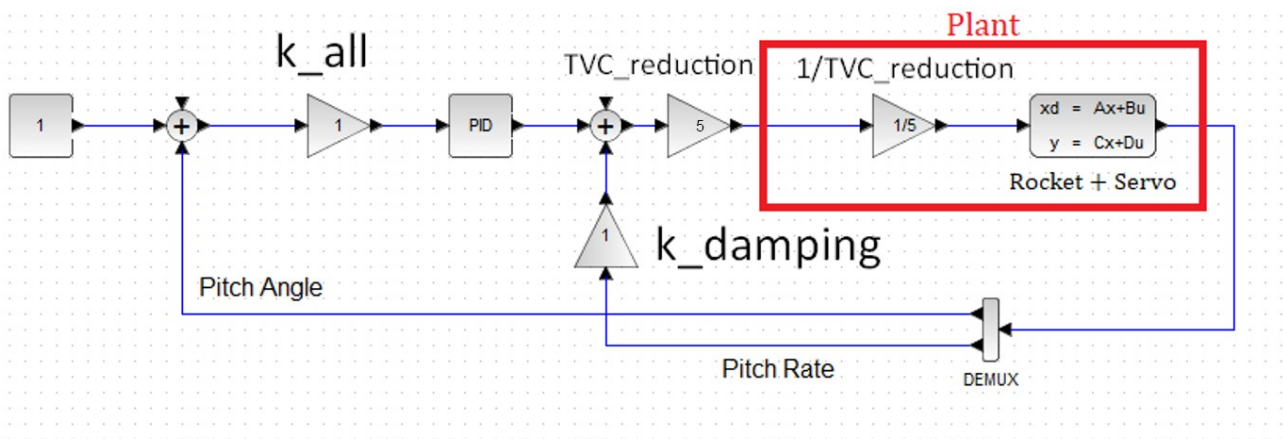


Figure 2.15 – Block diagram of the controller and model.

The user can choose between a step, ramp, or constant zero input based on the stability requirements for the system. This is allowed due to the non linearities present in the model, which may destabilize an otherwise stable system depending on the input.

After the program begins, the local accelerations are computed. The global velocity is transformed into the local frame, the accelerations are integrated and added to it, and lastly, the local velocity is once again transformed into the global frame. Once the new states and outputs are calculated, they are treated as readings from sensors and are manipulated by the PID, which computes a new input. This process is repeated at each time step of the simulation, ensuring that the flight is simulated from liftoff to burnout.

The reader should be careful when using the gains obtained by this method, since the flight computer code must match that of the simulator. Key points that should not be overlooked are:

- All angles are in radians, if not they are immediately converted, this means that both the input and the output of the controller are in radians. Angles in the GUI are in degrees to improve usability.
- The controller code is found in *control.py*.
- The output of the controller ($u_{controller}$) is multiplied by the TVC reduction ratio before being sent to the actuator, this must be implemented in the user's flight computer.

- If the user decides to implement anti-windup, its structure must be carefully emulated to ensure the same effects, mainly the saturation at the PID output, as well as after the $k_{damping}$ feedback.
- As for V1.1 of the simulator, where mass and moment of inertia are kept constant, the user should verify the gains obtained against the extremes of these parameters to ensure stability.
- The Torque Based Controller implemented simply multiplies the output of the controller by $\frac{Reference\ Thrust}{Current\ Thrust}$, and it is followed by another saturation to prevent over-deflection of the TVC mount. It is easy to see that if the current thrust is lower than the reference thrust, the gain is greater than unity, so as to produce the same torque output that the reference thrust would have generated.

3. Graphic Representation.

3.1 Colour of the Force Application Point in the Canvas.

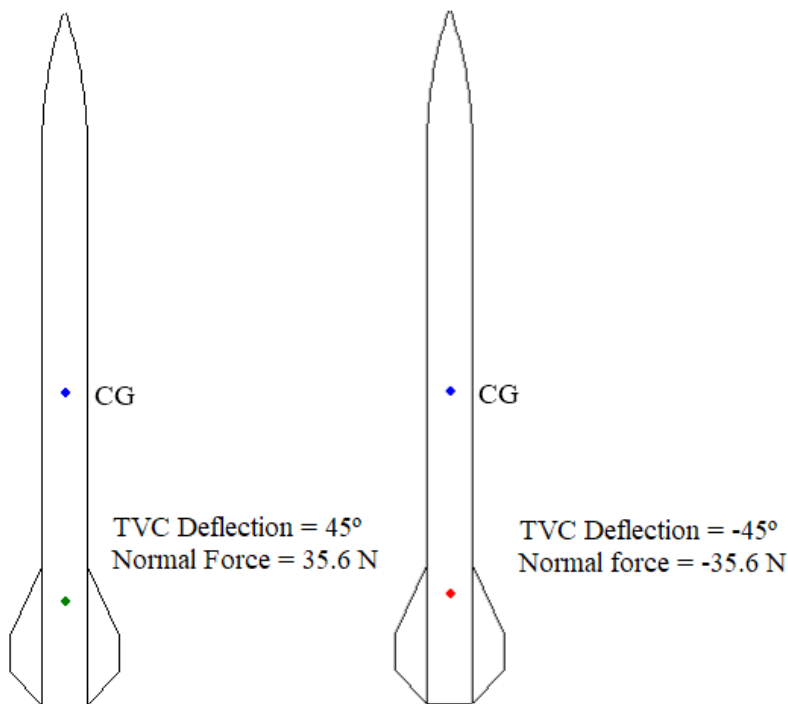


Figure 3.1: Example of the change in colour of the force application point.

The force application point is of colour red when the total normal force acting on the rocket is negative in z , and green when it is positive. Note that the total force includes the one produced by the deflection of the TVC mount.

3.2 Tridimensional Graphics.

The green arrow in Figure 3.2 represents the normal force of the passive aerodynamics, it does not include the effects of the control fin. The red arrow represents the normal force of the active component, be it the control fin or the TVC mount.

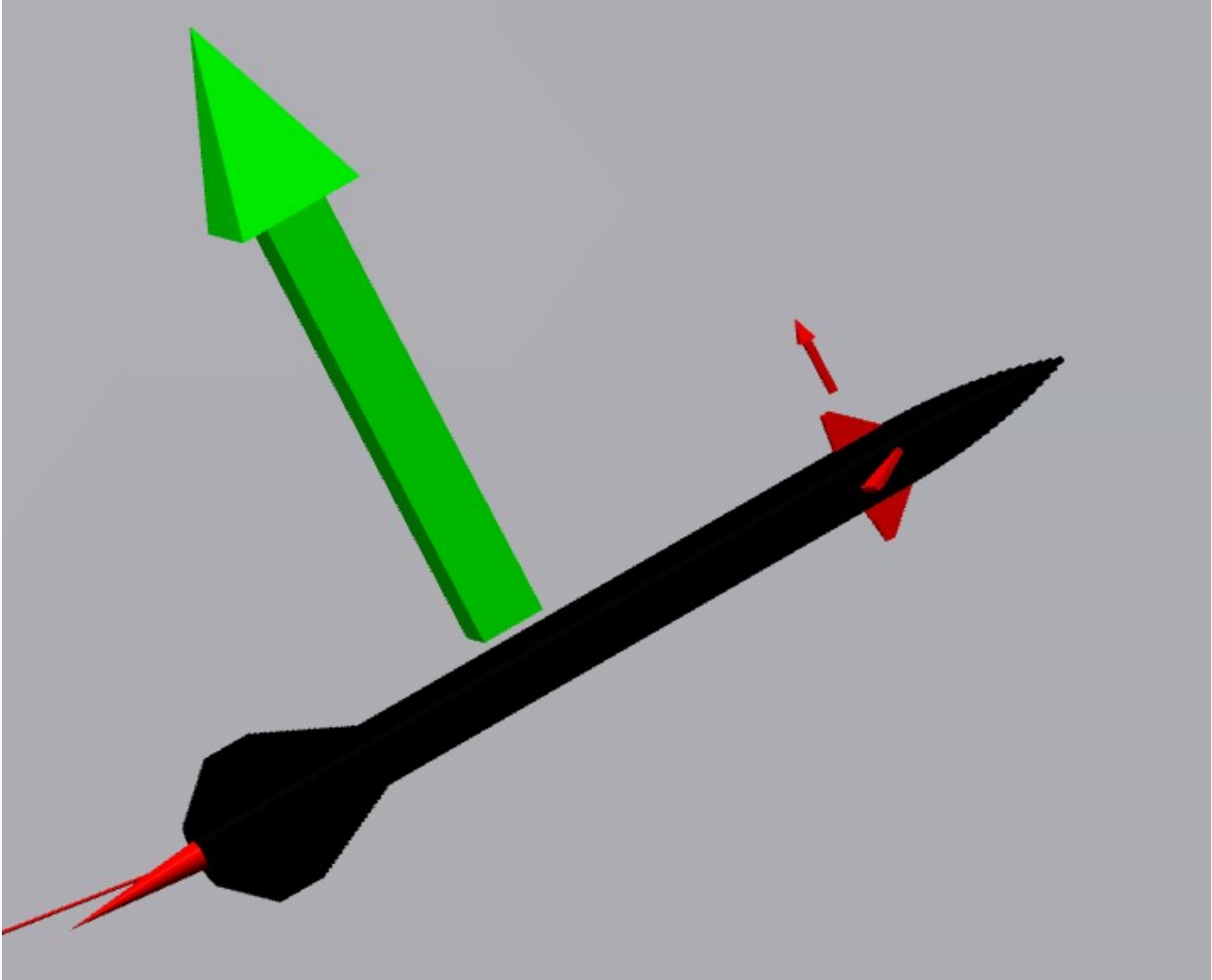


Figure 3.2: Tridimensional representation of the rocket's flight.

4. Conclusion.

The mathematical model of a model rocket has been developed and introduced into a simulator. In addition, the calculation of important aerodynamic parameters has been detailed.

The plug and play methodology has been achieved, due to the user only having to plug his rocket's parameters and play with the gains.

The 3D animation facilitates the analysis of the flight and the tuning of the controller.

Consequently, it is expected to improve the usability of the simulator.

Bibliography

- 1: Sampo Niskanen, Development of an Open Source model rocket simulation software., 2009
- 2: Barrowman J., Practical Calculation of the Aerodynamic Characteristics of Slender Finned Vehicles, 1967
- 3: Robert Galejs, Wind instability - What Barrowman left out.,
- 4: Robert E. Sheldahl, Paul C. Klimas, Aerodynamic Characteristics of Seven Symmetrical Airfoil Sections Through 180-Degree Angle of Attack for Use in Aerodynamic Analysis of Vertical Axis Wind Turbines, 1981
- 5: Perkins and Hage, Airplane Performance, Stability and Control,
- 6: Franklin W. Diederich, A PLAN-FORM PARAMETER FOR CORRELATING CERTAIN AERODYNAMIC CHARACTERISTICS OF SWEPT WINGS, 1951
- 7: Barrowman, J., The theoretical prediction of the center of pressure, 1966
- 8: Guido di Pasquo, Alexis M. Caratozzolo, Tomás Ziroldo, SG90 Characterization, 2019
- 9: Klaz, <https://dsp.stackexchange.com/questions/45042/bilinear-transformation-of-continuous-time-state-space-system>,